Journal of The Electrochemical Society, 2020 **167** 060528
1945-7111/2020/167(6)/060528/11/$40.00 © 2020 The Electrochemical Society ("ECS"). Published on behalf of ECS by IOP Publishing Limited

Analytical Modeling of Solid Phase Diffusion in Single-Layer and Composite Electrodes Under Time-Dependent Flux Boundary Condition

Mohammad Parhizi* and **Ankur Jain****,z

Mechanical and Aerospace Engineering Department, University of Texas at Arlington, Arlington, Texas, United States of America

Mathematical modeling of species diffusion in Li-ion cell electrodes is critical for improving performance and efficiency of electrochemical energy storage. There is a relative lack of literature in this direction for time-dependent flux boundary conditions. In this work, the method of Green's functions is used to solve the solid-phase diffusion problem in electrodes with a time-dependent flux boundary condition. While Green's functions have been used extensively for thermal transport problems, there is limited past work on application of Green's functions for solving species transport problems in electrochemical systems. The concentration distribution is first determined for a thin film electrode and spherical electrode particle. The method is then extended to determine the concentration profile in two-layer composite electrodes. The mathematical models presented in this work are validated by comparison with past studies and numerical simulations. Concentration profiles for a variety of time-dependent boundary conditions are presented. It is expected that improved understanding of diffusion under time-dependent flux boundary conditions may help improve the performance and efficiency of Li-ion based electrochemical energy storage devices and systems.
 [DOI: 10.1149/1945-7111/ab847c]

Manuscript submitted February 6, 2020; revised manuscript received March 14, 2020. Published April 14, 2020.

List of symbols

a	Length/radius of the inner layer (m)
b	Total lengthscale of the composite electrode (m)
c	non-dimensional concentration, C/C_{ref}
c_0	non-dimensional initial concentration
C_{ref}	reference concentration (mol m^{-3})
C	concentration (mol m^{-3})
D	diffusion coefficient (m^2s^{-1})
$F(x)$, $F(r)$	non-dimensional initial concentration
i	current (A)
l	ratio of the inner layer to the outer layer of the electrodes, $l = a/b$
t	non-dimensional time, $t = D\tau/b^2$
x	non-dimensional lengthscale, $x = X/b$
X	lengthscale (m)
R	radius (m)
r	non-dimensional radius, $r = R/b$
α	non-dimensional diffusion coefficient $\alpha = D_1/D_2$
δ	non-dimensional current density, $\delta = ib/nFDC_{ref}$ (F is the Faraday constant)
ε	frequency (1/s)
ω	non-dimensional frequency, $\omega = \varepsilon\, b^2/D$
τ	time (s)
λ	eigenvalues

Li-ion cells are the preferred electrochemical energy storage and conversion device in a wide variety of applications due to superior electrochemical characteristics compard to other secondary cells.[1–3] Higher power and energy density, longer cycle life and lower self-discharge rate are among the key advantages of Li-ion cells over competing technologies.[4–7]

A wide variety of mathematical models have been developed to predict and optimize electrochemical transport in a Li-ion cell under different operating conditions.[8,9] Mathematical models for Li-ion cells can broadly be divided into two categories—empirical and electrochemical models.[10,11] Empirical models employ data analysis techniques to predict the future state of a Li-ion cell based on past experimental data.[12,13] Compared to electrochemical models, empirical models are relatively faster and simpler, but cannot be used to determine finer details of electrochemical properties and cell characteristics. Alternatively, electrochemical models are more detailed, physics-based models that solve reaction kinetics, mass and charge transport equations.[8,14,15] Among the available physics-based models for Li-ion cells, Pseudo-2D model (P2D) and Single Particle Model (SPM) are the most popular ones.[8] P2D model solves for diffusion of Li-ions in the liquid electrolyte phase, as well as diffusion of Li-ions in solid particles and charge transport in both liquid and solid phases.[8,10] Diffusion of Li-ions in electrolyte and electronic conduction in both the liquid and solid phase are considered to occur in the linear dimension, x, while the diffusion of Li-ions in solid phase, assumed to be a spherical particle is considered to be a function of radial dimension, r within the solid particle, as well as x. Although P2D model is robust and accurate, the large number of equations needed to be solved significantly increases computational time.[16] Some work has been presented in simplification of computation associated with the P2D model.[16,17] In contrast, the SPM is a simplified, one-dimensional P2D model that describes only the solid phase diffusion of Li-ions in porous electrodes and neglects spatial variations in the electrolyte concentration and the potentials.[8,18,19] SPM is simple and computationally fast but limited to thin electrodes and applications with low discharge rates where the gradient in concentration of Li-ions in the liquid phase can be neglected and the porous electrode can be assumed to be a single particle.[16,20]

Mathematical models summarized above often result in a set of coupled equations that may be non-linear. As a result, exact solutions for these mathematical models exist only for a few limited cases. For example, diffusion equation for a solid solution cathodes initially at zero concentration has been solved using Laplace transformation approach.[21] Separation of Variables (SOV) technique has been used to solve a similar model for discharging of a Li-ion cell for different limiting cases.[22] Analytical solution for 1-D transient diffusion in a thin film, spherical electrode particle and composite electrode under galvanostatic discharge boundary condition and zero initial concentration has been developed using an extended separation of variables method.[23,24] Laplace transformation technique has been used to solve material balance equation in both solid and solution phases with non-zero initial concentration.[25] This model considers the migration term in solution phase diffusion with a constant transference number.[25] Integral transform method has been used to solve material balance equation for different cathode geometries under galvanostatic discharge boundary conditions.[26] A Finite Integral Transform (FIT) method has been used to find an exact solution for the diffusion of Li/Li+ into a spherical particle for arbitrary initial and boundary conditions.[27] The method of

*Electrochemical Society Student Member.
**Electrochemical Society Member.
zE-mail: jaina@uta.edu

Pseudo-Steady-State (PSS) is used to ensure convergence in this work.[27] Green's function approach has been used to solve the material balance equation in solution phase of a thin film electrode under a galvanostatic discharge condition.[28]

In addition to the limited cases where an exact solution is possible, approximate analytical solutions have also been developed in order to reduce the complexity and required computational time. An example is the Parabolic Profile approximation (PP) method, in which the concentration profile in a spherical electrode particle is assumed to be a second, fourth, or sixth order polynomial.[29,30] Other approximate analytical methods include residue grouping technique which is based on the transcendental transfer function approach,[31] State Variable Model (SVM), which is a combination of analytical transfer functions and a numerical transfer matrix,[31,32] Electrode Averaged Model (EAM),[33] Proper Orthogonal Decomposition (POD),[34] Extended Single Particle Model (ESPM),[35,36] etc.

While most of the past analytical models focus on constant galvanostatic discharge conditions, there is a relative lack of work on time-dependent flux boundary conditions. For example, the diffusion problem in composite electrode has been solved for a constant boundary condition.[23] However, in some cases, time-dependent boundary conditions are also important since the applied current density may be time-dependent. While several past studies presented approximate solutions to such problems,[15,16,37,38] there is a relative lack of analytical solutions for this class of problems. The few analytical solutions that have been presented for such problems are for the case of single-layer electrodes, and not composite electrodes.[27] For example, exact solutions for diffusion in a spherical single electrode particle has been presented using the finite integral transform method for time-dependent boundary conditions.[27] Green's function is a powerful tool for solving such problems. While the use of Green's functions in heat transfer problems is quite common,[39,40] only limited work exists on the use of this tool for species diffusion problems in electrochemical systems.[28]

This paper presents an exact analytical solution for Li-ion diffusion in thin film and spherical electrodes, as well as composite two-layer electrodes with arbitrary initial conditions and time-dependent flux boundary condition using Green's function approach. The exact solution presented here is validated against both numerical simulations and previous studies. Concentration distribution for cases representative of realistic discharge conditions is predicted using the model. The mathematical tools developed in this work help understand species transport in a Li-ion cell, thereby contributing towards improved performance of electrochemical energy storage devices and systems.

Mathematical Modeling

Green's function solution.—Greens' function is a powerful mathematical tool which can be used to solve linear partial differential equations with multiple non-homogeneities in the governing equation, boundary conditions and initial condition.[39,40] While the method of separation of variables is not applicable to problems with time-dependent non-homogeneities, Green's function approach can be used to solve a wide variety of such problems. Green's function approach has been used for a wide variety of thermal conduction problems.[39,40] Since thermal and species diffusion are governed by similar conservation equations, Green's function approach can also be used for solving species diffusion problems, such as those that appear in Li-ion cell electrodes.

The general form of the solution to the 1-D diffusion problem presented here in non-dimensional form using Green's function approach is given by[39]:

$$c(x,\,t) = \int G(x,\,t|x',\,t')_{t'=0} F(x') x'^{p} dx' + \iint G(x,\,t|x',\,t') g(x',\,t') x'^{p} dx' dt' + \sum_{i=1}^{N} \left\{ \int [x'^{p} G(x,\,t|x',\,t')]_{x=x'} f_i(t') dt' \right\} \quad [1]$$

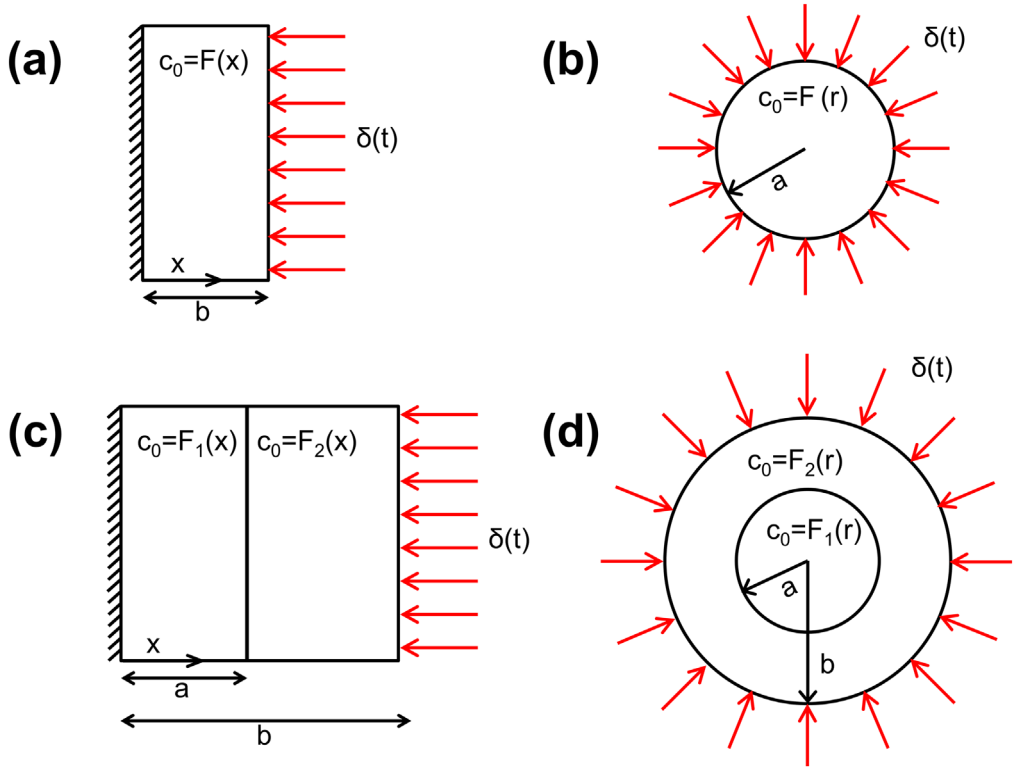

Figure 1. Schematic of the four electrode geometries considered in this work: (a) Thin film electrode; (b) Spherical electrode particle; (c) Composite slab electrode; (d) Composite spherical electrode.

Where x'^{p} is the Sturm–Liouville weight function, and $p = 0$, 1 and 2 for slabs, cylinders and spheres respectively. Here, $F(x)$ is the initial condition and g is the generation or consumption term. The summation is taken over all boundaries of the problem. G is the Green's function that must be determined.

The three terms on the right-hand side of Eq. 1 represent contributions of the initial concentration, generation or consumption, and boundary conditions respectively. In order to present the solution given by Eq. 1 for a specific problem, the Green's function, $G(x, t|x', t')$ needs to be determined first. This is usually done by solving the corresponding homogeneous version of the problem. For any homogeneous problem, the second and third term in Eq. 1 will be zero. Therefore, a comparison between the solution to the homogeneous problem and the first term in Eq. 1 provides the Green's function evaluated at $t' = 0$, $G(x, t|x', t')_{t'=0}$. The full Green's function, $G(x, t|x', t')$ is then determined by replacing t with $(t - t')$ in $G(x, t|x', t')_{t'=0}$.

Analytical solutions for transient diffusion under a time-dependent flux condition using Green's function approach are presented next. A number of progressively complicated cases are considered—a thin film electrode, a spherical particle electrode and composite electrodes, both Cartesian and spherical. Figures 1a–1d show schematics of the thin film, spherical particle, two layer and spherical composite electrodes respectively. Specific details for these cases are discussed in sub-sections below.

Thin film electrode.—Figure 1a shows a schematic of a one-dimensional thin film electrode initially at a non-uniform concentration of $F(x)$ and operating under a time-dependent flux boundary condition. Referring to the non-dimensionalization scheme presented in the Nomenclature section, the governing equation for concentration distribution can be written in non-dimensional form as follows:

$$\frac{\partial^2 c}{\partial x^2} = \frac{\partial c}{\partial t} \qquad [2]$$

Associated boundary conditions at the two ends are

$$\left(\frac{\partial c}{\partial x}\right)_{x=0} = 0 \quad \text{at } x = 0 \qquad [3]$$

$$\left(\frac{\partial c}{\partial x}\right)_{x=1} = \delta(t) \quad \text{at } x = 1 \qquad [4]$$

Equation 3 results from symmetry at $x = 0$ and Eq. 4 represents the applied, time-dependent flux boundary condition at $x = 1$, where $\delta(t)$ is the dimensionless current density.where δ is the dimensionless, time-dependent current density defined in the nomenclature section.

The initial condition associated with this problems is:

$$c = F(x) \quad \text{at } t = 0 \qquad [5]$$

As outlined in the previous sub-section, the first step to construct the Green's function associated with this problem is to solve the corresponding homogeneous problem. The solution to the homogeneous problem can be determined using the Separation of Variables technique[39] as follows:

$$c(x, t) = \int_0^1 F(x')dx' + \int_0^1 \sum_{n=1}^{\infty} [2\cos(\lambda_n x)\cos(\lambda_n x')\exp(-\lambda_n^2 t)]F(x')dx' \qquad [6]$$

where $\lambda_n = n\pi$ are the eigenvalues for $n = 1, 2, 3, \ldots$. A comparison between Eqs. 1 and 6 indicates that the expression for Green's function calculated for $t' = 0$ can be written as follows:

$$G(x, t|x', t')_{t'=0} = 1 + 2\sum_{n=1}^{\infty} \cos(\lambda_n x)\cos(\lambda_n x')\exp(-\lambda_n^2 t) \qquad [7]$$

Therefore, the general form of the Green's function is obtained by replacing t with $t - t'$ in Eq. 7:

$$G(x, t|x', t') = 1 + 2\sum_{n=1}^{\infty} \cos(\lambda_n x)\cos(\lambda_n x')\exp(-\lambda_n^2 (t - t')) \qquad [8]$$

Now that the Green's function is determined, a solution for the problem defined in Eqs. 2–5 can be constructed. The solution can be written as:

$$c(x, t) = c_1(x, t) + c_2(x, t) + c_3(x, t) \qquad [9]$$

where

$$c_1(x, t) = \int_{x'=0}^{1} F(x')dx' + \int_{x'=0}^{1} \sum_{n=1}^{\infty} [2\cos(\lambda_n x)\cos(\lambda_n x')\exp(-\lambda_n^2 t)]F(x')dx' \qquad [10]$$

$$c_2(x, t) = 0 \qquad [11]$$

$$c_3(x, t) = \int_{t'=0}^{t} \delta(t')dt' + 2\sum_{n=1}^{\infty} \cos(\lambda_n x)\cos(\lambda_n) \times \int_{t'=0}^{t} \exp(-\lambda_n^2 (t - t'))\delta(t')dt' \qquad [12]$$

Note that the solution accounts for the time-dependent flux boundary condition in the expression for $c_3(x, t)$, given by Eq. 12. Further, since there is no non-homogeneity in Eq. 2, the second term of the Green's function solution is zero.

As a special case, if the initial concentration is constant, C_0, the second term in Eq. 10 becomes zero, leading to further simplification.

Spherical electrode particle.—Figure 1b shows a schematic of a one-dimensional spherical particle initially at a given concentration distribution $F(r)$ and subject to time-dependent flux at its surface. The non-dimensional governing equation for concentration distribution and boundary conditions can be written in non-dimensional form as follows:

$$\frac{1}{r^2}\frac{\partial}{\partial r}\left(r^2\frac{\partial c}{\partial r}\right) = \frac{\partial c}{\partial t} \qquad [13]$$

where the initial and boundary conditions are

$$c = F(r) \quad \text{at } t = 0 \qquad [14]$$

$$c \Rightarrow \textit{finite} \quad \text{as } r \to 0 \qquad [15]$$

$$\left(\frac{\partial c}{\partial r}\right)_{r=1} = \delta(t) \quad \text{at } r = 1 \qquad [16]$$

Similar to the thin film electrode problem, the homogeneous problem must be solved first. In order to do so, a new variable U is defined as $U(r, t) = rc(r, t)$, which facilitates a solution of the homogeneous problem using separation of variables method. The concentration profile can be derived to be:

$$c(r,\,t) = 3\int_0^1 r'^2F(r)dr' + \int_0^1 \sum_{n=1}^{\infty}\left[\frac{1}{N_n rr'}\sin(\lambda_n r)\sin(\lambda_n r')\exp(-\lambda_n^2 t)r'^2F(r')dr'\right] \quad [17]$$

where N_n is the norm defined as $N_n = \frac{\lambda_n^2}{2(\lambda_n^2+1)}$, and the eigenvalues λ_n are positive roots of the transcendental equation $\lambda_n \cot \lambda_n = 1$.

Thus, comparing Eq. 17 with Eq. 1 and taking $p = 2$ for the case of a sphere, the Green's function calculated at $t' = 0$ can be determined as follows:

$$G(r,\,t|r',\,t')_{t'=0} = 3 + \sum_{n=1}^{\infty}\frac{1}{N_n rr'}\sin(\lambda_n r)\sin(\lambda_n r')\exp(-\lambda_n^2 t) \quad [18]$$

The complete form of Green's function can be obtained by obtained by replacing t with $(t - t')$ in Eq. 18.

$$G(r,\,t|r',\,t') = 3 + \sum_{n=1}^{\infty}\frac{1}{N_n rr'}\sin(\lambda_n r)\sin(\lambda_n r')\exp(-\lambda_n^2 (t-t')) \quad [19]$$

Thus, based on Eq. 1, the concentration profile for the original problem can be written as:

$$c(r,\,t) = c_1(r,\,t) + c_2(r,\,t) + c_3(r,\,t) \quad [20]$$

where

$$c_1(r,\,t) = 3\int_{r'=0}^1 r'^2F(r')dr' + \int_0^1\sum_{n=1}^{\infty}\left[\frac{1}{N_n rr'}\sin(\lambda_n r)\sin(\lambda_n r')\exp(-\lambda_n^2 t)\right]r'^2F(r')dr' \quad [21]$$

$$c_2(r,\,t) = 0 \quad [22]$$

$$c_3(r,\,t) = 3\int_{t'=0}^t \delta(t')dt' + \frac{1}{r}\sum_{n=1}^{\infty}\frac{1}{N_n}\sin(\lambda_n r)\sin(\lambda_n) \times \int_{t'=0}^t \exp(-\lambda_n^2(t-t'))\delta(t')dt' \quad [23]$$

Similar to the previous problem, the third component of the solution contains various integrals of the time-dependent flux boundary condition. Note that $c_2(x,\,t)$ becomes zero since there is no non-homogeneity in Eq. 13.

Composite electrodes.—This section presents solutions for composite electrodes under time-dependent flux boundary condition. After a brief introduction on Green's function for multi-layer problems, the solutions for a two-layer composite electrode in a rectangular geometry and a composite spherical electrode particle will be presented.

Green's function approach can be used to solve multilayer problems. While the general procedure is similar to single-layer problems discussed in previous sections, the derivation of the solution is somewhat more complicated. Green's function solution for an M-layer problem involving non-homogeneities in the governing equation and boundary conditions can be written as[39]:

$$c_i(x,\,t) = \sum_{j=1}^{M}\left[\int_{x'=x_j}^{x_{j+1}} G_{ij}(x,\,t|x',\,t')_{t'=0}\cdot F_j(x')x'^p dx' + \int_{t'=0}^{t}\int_{x'=x_j}^{x_{j+1}} G_{ij}(x,\,t|x',\,t')g_j(x',\,t')x'^p dx'dt' + \int_{t'=0}^{t}[x'^p G_{ij}(x,\,t|x',\,t')]_{x'=x_j}\cdot f_j(t')dt'\right] \quad [24]$$

where $i = 1, 2,\ldots, M$ and $p = 0$, 1 and 2 for slabs, cylinders and spheres, respectively

The composite Green's function is defined as[39]:

$$G_{ij}(x,\,t|x',\,t')_{t'=0} = \sum_{n=1}^{\infty}\frac{1}{N_n}\Gamma(t)\psi_{in}(x)\psi_{jn}(x') \quad [25]$$

$$G_{ij}(x,\,t|x',\,t') = \sum_{n=1}^{\infty}\frac{1}{N_n}\Gamma(t-t')\psi_{in}(x)\psi_{jn}(x') \quad [26]$$

where x'^p is the Sturm–Liouville weight function. N_n is the norm, given by

$$N_n = \sum_{j=1}^{M}\int_{x'=x_j}^{x_{j+1}} x'^p\psi_{jn}^2(x')dx' \quad [27]$$

where $\Gamma(t)$ and $\psi(x)$ can be found by solving the corresponding homogeneous problem, as discussed next.

Two-layer composite electrode.—Figure 1c shows a two-layer composite electrode with an initial concentration distribution given by $F_1(x)$ and $F_2(x)$ in the two layers, respectively. The two layers have diffusion coefficient of D_1 and D_2, respectively. The goal is to find the concentration profile in the two regions. The governing equation, initial and boundary conditions can be written in non-dimensional form as follows:

$$\frac{\partial^2 c_1}{\partial x^2} = \frac{1}{\alpha}\frac{\partial c_1}{\partial t} \quad 0 < x < l \quad [28]$$

$$\frac{\partial^2 c_2}{\partial x^2} = \frac{\partial c_2}{\partial t} \quad l < x < 1 \quad [29]$$

Subject to the following boundary conditions

$$\left(\frac{\partial c_1}{\partial x}\right)_{x=0} = 0 \quad \text{at } x = 0 \quad [30]$$

$$c_1 = c_2 \quad \text{at } x = l \quad [31]$$

$$\alpha\left(\frac{\partial c_1}{\partial x}\right)_{x=l} = \left(\frac{\partial c_2}{\partial x}\right)_{x=l} \quad \text{at } x = l \quad [32]$$

$$\left(\frac{\partial c_2}{\partial x}\right)_{x=1} = \delta(t) \quad \text{at } x = 1 \qquad [33]$$

Equation 30 arises from symmetry at $x = 0$. Equations 31 and 32 are interfacial conditions representing species continuity and conservation of flux, respectively. Equation 33 is the applied time-dependent boundary condition.

The initial condition is

$$c_1 = F_1(x) \quad \text{at } t = 0 \qquad [34]$$

$$c_2 = F_2(x) \quad \text{at } t = 0 \qquad [35]$$

where F_1 and F_2 are the non-dimensional initial conditions.

Note the presence of additional non-dimensional parameters in this problem due to the presence of two layers that, in general, may have different thicknesses and diffusion coefficients.

This problem is considerably more complicated than the ones discussed in previous two sub-sections. However, the same concept of developing a Green's function solution can be applied, starting with derivation of a solution of the corresponding homogeneous problem. Similar to the separation of variables method for single-layer problems, the solution can be written as

$$c_i(x, t) = \psi_i(x)\Gamma(t) \qquad [36]$$

Where $i = 1, 2$.

Substituting Eq. 36 back into the governing equations results in two separate differential equations which can be solved for time-dependent and space-dependent components of Eq. 36 as follows:

$$\Gamma_n(t) = \exp(-\lambda_n^2 t) \qquad [37]$$

$$\psi_{1n}(x) = A_{1n}\sin\left(\frac{\lambda_n x}{\sqrt{\alpha}}\right) + B_{1n}\cos\left(\frac{\lambda_n x}{\sqrt{\alpha}}\right) \qquad [38]$$

$$\psi_{2n}(x) = A_{2n}\sin(\lambda_n x) + B_{2n}\cos(\lambda_n x) \qquad [39]$$

Note that the non-dimensional parameter α is absorbed in the solution of one of the layers. Applying boundary conditions results in a set of equations for the unknown coefficients A_{in} and B_{in} written in matrix form as follows:

$$\begin{bmatrix} 1 & 0 & 0 & 0 \\ 0 & \cos\frac{\lambda_n l}{\sqrt{\alpha}} & -\sin\lambda_n l & -\cos\lambda_n l \\ 0 & \sqrt{\alpha}\sin\frac{\lambda_n l}{\sqrt{\alpha}} & \cos\lambda_n l & -\sin\lambda_n l \\ 0 & 0 & \cos\lambda_n & -\sin\lambda_n \end{bmatrix} \begin{bmatrix} A_{1n} \\ B_{1n} \\ A_{2n} \\ B_{2n} \end{bmatrix} = \begin{bmatrix} 0 \\ 0 \\ 0 \\ 0 \end{bmatrix} \qquad [40]$$

In order to determine the eigenvalues, λ_n, Eq. 40 may be required to result in a nontrivial solution. This implies that the determinant of the matrix in Eq. 40 must be equal to zero, thereby resulting in a transcendental equation for the eigenvalues as follows:

$$\tan(\lambda_n l - \lambda_n) - \sqrt{\alpha}\tan\left(\frac{\lambda_n}{\sqrt{\alpha}}\right) = 0 \qquad [41]$$

Without loss of generality, any one of the non-vanishing coefficients in Eq. 44 may be set to unity. In this case, B_{1n} is chosen to be equal to 1. Consequently, the coefficients, A_{in} and B_{in}, are determined to be

$$A_{1n} = 0 \qquad [42]$$

$$B_{1n} = 1 \qquad [43]$$

$$A_{2n} = \cos\frac{\lambda_n l}{\sqrt{\alpha}}\sin\lambda_n l - \sqrt{\alpha}\sin\frac{\lambda_n l}{\sqrt{\alpha}}\cos\lambda_n l \qquad [44]$$

$$B_{2n} = \cos\frac{\lambda_n l}{\sqrt{\alpha}}\cos\lambda_n l + \sqrt{\alpha}\sin\frac{\lambda_n l}{\sqrt{\alpha}}\sin\lambda_n l \qquad [45]$$

With these values, all the information is available to construct Green's functions based on Eqs. 25 and 26. The concentration profile in each layer is found to be

$$\begin{aligned} c_1(x, t) = &\sum_{n=0}^{\infty}\int_{x'=0}^{x'=l}\frac{1}{N_n}\exp(-\lambda_n^2 t)\cos\left(\frac{\lambda_n x}{\sqrt{\alpha}}\right)\cos\left(\frac{\lambda_n x'}{\sqrt{\alpha}}\right)F_1(x')dx' \\ &+ \int_{x'=l}^{x'=1}\frac{1}{N_n}\exp(-\lambda_n^2 t)\cos\left(\frac{\lambda_n x}{\sqrt{\alpha}}\right)(A_{2n}\sin(\lambda_n x') + B_{2n}\cos(\lambda_n x'))F_2(x')dx' \\ &+ \int_{t'=0}^{t'=t}\frac{1}{N_n}\exp(-\lambda_n^2(t-t'))\cos\left(\frac{\lambda_n x}{\sqrt{\alpha}}\right)(A_{2n}\sin(\lambda_n) + B_{2n}\cos(\lambda_n))\delta(t')dt' \end{aligned} \qquad [46]$$

$$\begin{aligned} c_2(x, t) = &\sum_{n=0}^{\infty}\int_{x'=0}^{x'=l}\frac{1}{N_n}\exp(-\lambda_n^2 t) \\ &\times (A_{2n}\sin(\lambda_n x) + B_{2n}\cos(\lambda_n x))\cos\left(\frac{\lambda_n x'}{\sqrt{\alpha}}\right)F_1(x')dx' \\ &+ \int_{x'=l}^{x'=1}\frac{1}{N_n}\exp(-\lambda_n^2 t)(A_{2n}\sin(\lambda_n x) + B_{2n}\cos(\lambda_n x)) \\ &\times (A_{2n}\sin(\lambda_n x') + B_{2n}\cos(\lambda_n x'))F_2(x')dx' \\ &+ \int_{t'=0}^{t'=t}\frac{1}{N_n}\exp(-\lambda_n^2(t-t'))(A_{2n}\sin(\lambda_n x) + B_{2n}\cos(\lambda_n x)) \\ &\times (A_{2n}\sin(\lambda_n) + B_{2n}\cos(\lambda_n))\delta(t')dt' \end{aligned} \qquad [47]$$

Where A_{2n} and B_{2n} are shown in Eqs. 44 and 45 and N_n is defined in Eq. 27. Note that the zeroth terms of Eqs. 46 and 47 can be calculated by finding the limits of these equations as $\lambda \to 0$. For a special case of zero initial concentration in both layers and constant flux, the solution can be written as follows:

$$c_1(x, t) = \delta \cdot t + \sum_{n=1}^{\infty} \int_{t'=0}^{t'=t} \frac{1}{N_n} \exp\left(-\lambda_n^2 (t - t')\right) \times \cos\left(\frac{\lambda_n x}{\sqrt{\alpha}}\right)(A_{2n} \sin(\lambda_n) + B_{2n} \cos(\lambda_n))\delta(t')dt' \quad [48]$$

$$c_2(x, t) = \delta \cdot t + \sum_{n=1}^{\infty} \int_{t'=0}^{t'=t} \frac{1}{N_n} \exp\left(-\lambda_n^2 (t - t')\right) \times (A_{2n} \sin(\lambda_n x) + B_{2n} \cos(\lambda_n x)) \times (A_{2n} \sin(\lambda_n) + B_{2n} \cos(\lambda_n))\delta(t')dt' \quad [49]$$

Diffusion in a two-layer spherical composite electrode is analyzed next.

Spherical composite electrode.—Figure 1d presents a schematic of a composite spherical electrode. Similar to the previous subsection, the initial concentration in the two layers is assumed to be $F_1(r)$ and $F_2(r)$, respectively. A time-varying, inward flux $\delta(t)$ is assumed at the outer surface. In this case, the governing equation, initial and boundary conditions can be written as follows:

$$\frac{1}{r^2}\frac{\partial}{\partial r}\left(r^2 \frac{\partial c}{\partial r}\right) = \frac{1}{\alpha}\frac{\partial c_1}{\partial t} \quad 0 < x < l \quad [50]$$

$$\frac{1}{r^2}\frac{\partial}{\partial r}\left(r^2 \frac{\partial c}{\partial r}\right) = \frac{\partial c_2}{\partial t} \quad l < x < 1 \quad [51]$$

Subject to the following boundary conditions

$$c \Rightarrow finite \quad \text{as } r \to 0 \quad [52]$$

$$c_1 = c_2 \quad \text{at } r = l \quad [53]$$

$$\alpha\left(\frac{\partial c_1}{\partial r}\right)_{r=l} = \left(\frac{\partial c_2}{\partial r}\right)_{r=l} \quad \text{at } r = l \quad [54]$$

$$\left(\frac{\partial c_2}{\partial r}\right)_{r=1} = \delta(t) \quad \text{at } r = 1 \quad [55]$$

and the initial conditions

$$c_1 = F_1(r) \quad \text{at } t = 0 \quad [56]$$

$$c_2 = F_2(r) \quad \text{at } t = 0 \quad [57]$$

Here, Eq. 53 an 54 represent species continuity and flux conservation, respectively, at the interface.

Similar to the single spherical particle problem, a new variable U is defined as $U_i(r, t) = rc_i(r, t)$, to facilitate the derivation. After re-writing the governing equations and boundary conditions based on the new variable, U, and employing the separation of variables technique, the solution to the homogeneous problem can be written as:

$$c_i(x, t) = r\psi_i(r)\Gamma(t) \quad [58]$$

$$\Gamma_n(t) = \exp\left(-\lambda_n^2 t\right) \quad [59]$$

$$\psi_{1n}(r) = A_{1n} \sin\left(\frac{\lambda_n r}{\sqrt{\alpha}}\right) + B_{1n} \cos\left(\frac{\lambda_n r}{\sqrt{\alpha}}\right) \quad [60]$$

$$\psi_{2n}(r) = A_{2n} \sin(\lambda_n r) + B_{2n} \cos \lambda_n r \quad [61]$$

Substituting Eqs. 60 and 61 back into the boundary conditions results in the following equations in matrix form

$$\begin{bmatrix} \sin\frac{\lambda_n l}{\sqrt{\alpha}} & 0 & -\sin\lambda_n l & -\cos\lambda_n l \\ 0 & 1 & 0 & 0 \\ \alpha\left(\frac{\lambda_n l}{\sqrt{\alpha}}\cos\frac{\lambda_n l}{\sqrt{\alpha}} - \sin\frac{\lambda_n l}{\sqrt{\alpha}}\right) & 0 & \sin\lambda_n l - \lambda_n l\cos\lambda_n l & \cos\lambda_n l + \lambda_n l\sin\lambda_n l \\ 0 & 0 & \lambda_n\cos\lambda_n - \sin\lambda_n & \lambda_n\sin\lambda_n + \cos\lambda_n \end{bmatrix} \begin{bmatrix} A_{1n} \\ B_{1n} \\ A_{2n} \\ B_{2n} \end{bmatrix} = \begin{bmatrix} 0 \\ 0 \\ 0 \\ 0 \end{bmatrix} \quad [62]$$

Similar to the previous section, one of the non-zero coefficients, A_{1n} is set to a value of 1. Therefore, the coefficients, A_{in} and B_{in}, are determined to be

$$A_{1n} = 1 \quad [63]$$

$$B_{1n} = 0 \quad [64]$$

$$A_{2n} = \frac{1}{\lambda_n l}\left(\sin\frac{\lambda_n l}{\sqrt{\alpha}}(\cos\lambda_n l + \lambda_n l\sin\lambda_n l) - \alpha\cos\lambda_n l\left(\sin\frac{\lambda_n l}{\sqrt{\alpha}} - \frac{\lambda_n l}{\sqrt{\alpha}}\cos\frac{\lambda_n l}{\sqrt{\alpha}}\right)\right) \quad [65]$$

$$B_{2n} = \frac{1}{\lambda_n l}\left(\alpha\sin\lambda_n l\left(\sin\frac{\lambda_n l}{\sqrt{\alpha}} - \frac{\lambda_n l}{\sqrt{\alpha}}\cos\frac{\lambda_n l}{\sqrt{\alpha}}\right) - \sin\frac{\lambda_n l}{\sqrt{\alpha}}(\sin\lambda_n l - \lambda_n l\cos\lambda_n l)\right) \quad [66]$$

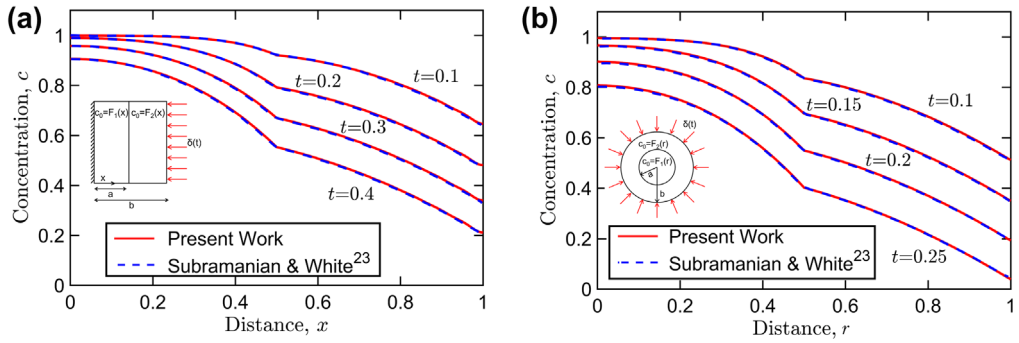

Figure 2. Validation against past study[23] for composite two-layer electrodes: Non-dimensional concentration as a function of non-dimensional distance, x and r, at multiple times for (a) A composite slab electrode, (b) A composite spherical electrode. Both cases are for discharge, with $\delta = -1$.

Based on the requirement of non-trivial solution of Eq. 62, the eigenvalues, λ_n are determined to be given by the roots of the following transcendental equation

$$\tan\frac{\lambda_n l}{\sqrt{\alpha}}\tan(\lambda_n l-\lambda_n)(\alpha-1-\lambda_n^2 l)+\tan\frac{\lambda_n l}{\sqrt{\alpha}}(\lambda_n l-\lambda_n+\alpha\lambda_n)-\alpha\frac{\lambda_n l}{\sqrt{\alpha}}\tan(\lambda_n l-\lambda_n)-\alpha\frac{\lambda_n^2 l}{\sqrt{\alpha}}=0 \quad [67]$$

Based on these expressions for the coefficients, the concentration profile can be determined in both spherical regions from the following equations:

$$\begin{aligned}c_1(x,t)=&\sum_{n=0}^{\infty}\int_{r=0}^{r'=l}\frac{r'1}{rN_n}\exp(-\lambda_n^2 t)\sin\left(\frac{\lambda_n r}{\sqrt{\alpha}}\right)\times\sin\left(\frac{\lambda_n r'}{\sqrt{\alpha}}\right)F_1(r')dx'\\&+\int_{r'=1}^{r'=l}\frac{r'}{rN_n}\exp(-\lambda_n^2 t)\sin\left(\frac{\lambda_n r}{\sqrt{\alpha}}\right)\times(A_{2n}\sin(\lambda_n r')+B_{2n}\cos(\lambda_n r'))F_2(r')dr'\\&+\int_{t'=t}^{t'=0}\frac{l}{rN_n}\exp(-\lambda_n^2(t-t'))\sin\left(\frac{\lambda_n r}{\sqrt{\alpha}}\right)\times(A_{2n}\sin(\lambda_n)+B_{2n}\cos(\lambda_n))\delta(t')dt'\end{aligned} \quad [68]$$

$$\begin{aligned}c_2(x,t)=&\sum_{n=0}^{\infty}\int_{r'=0}^{r'=l}\frac{r'}{rN_n}\exp(-\lambda_n^2 t)\times(A_{2n}\sin(\lambda_n r)+B_{2n}\cos(\lambda_n r))\times\sin\left(\frac{\lambda_n r'}{\sqrt{\alpha}}\right)F_1(r')dr'\\&+\int_{r'=l}^{r'=1}\frac{r'}{rN_n}\exp(-\lambda_n^2 t)\times(A_{2n}\sin(\lambda_n r)+B_{2n}\cos(\lambda_n r))\times(A_{2n}\sin(\lambda_n r')+B_{2n}\cos(\lambda_n r'))F_2(r')dr'\\&+\int_{t'=0}^{t'=t}\frac{l}{rN_n}\exp(-\lambda_n^2(t-t'))(A_{2n}\sin(\lambda_n r)+B_{2n}\cos(\lambda_n r))(A_{2n}\sin(\lambda_n)+B_{2n}\cos(\lambda_n))\delta(t')dt'\end{aligned} \quad [69]$$

Note that the zeroth terms of Eqs. 68 and 69 can be calculated by finding the limits of these equations as $\lambda \to 0$. Moreover, in order to calculate the concentration at $r = 0$, one must calculate the limit when $r \to 0$. In a simple case of zero concentration in both layers and constant flux, the solution can be written as follows:

$$c_1(x,t)=3\delta\cdot t+\sum_{n=0}^{\infty}\int_{t'=0}^{t'=t}\frac{l}{rN_n}\exp(-\lambda_n^2(t-t'))\times\sin\left(\frac{\lambda_n r}{\sqrt{\alpha}}\right)(A_{2n}\sin(\lambda_n)+B_{2n}\cos(\lambda_n))\delta(t')dt' \quad [70]$$

$$c_2(x,t)=3\delta\cdot t+\sum_{n=0}^{\infty}\int_{t'=0}^{t'=t}\frac{l}{rN_n}\exp(-\lambda_n^2(t-t'))\times(A_{2n}\sin(\lambda_n r)+B_{2n}\cos(\lambda_n r))\times(A_{2n}\sin(\lambda_n)+B_{2n}\cos(\lambda_n))\delta(t')dt' \quad [71]$$

Results and Discussion

Model validation.—Validation of the Green's function based models presented in the mathematical modeling section is carried out by comparison with past studies and numerical computation. This comparison is discussed in the follwoing sections, below.

Validation against past studies.—Concentration profiles predicted by the Green's function based models are compared against past studies by Subramanian & White[23] and Guo & White.[37] While Subramanian & White[23] used the method of separation of variables for composite electrodes under a galvanostatic boundary condition, Guo & White[37] used an approximate analytical solution for spherical electrode particle under both constant and a time-dependent flux boundary conditions.

For comparison with Subramanian & White,[23] the cases of galvanostatic discharge boundary condition for both thin film composite electrodes and composite spherical electrode particle are considered. The dimensionless current density, δ, and ratio of diffusion coefficients, α, are taken to be 1 and 0.25, respectively, consistent with Subramanian & White.[23] Thicknesses of both layers are considered to be equal. Figure 2a plots the concentration profile determined by the present model and previous work[23] for a composite slab. Similar comparison is presented in Fig. 2b for a composite spherical electrode. In both cases, results show very good agreement between the present model and past studies across the entire electrode and at multiple times.

In order to further validate the Green's function model, a study by Guo & White[37] is used for comparison. This paper presented an approximate analytical solution for solid-phase diffusion in a spherical particle under constant and time-dependent flux boundary condition. Values of various parameters are taken to be consistent with the previous work. Figure 3 presents a plot of concentration as a function of time at the surface of the electrode for a constant dimensionless current density of $\delta = 0.2$. Very good agreement between the present work and past work is seen.

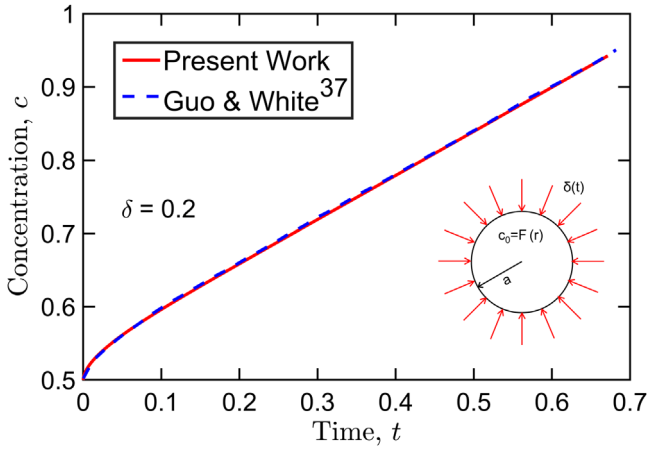

Figure 3. Validation against past study[37] for a spherical particle electrode: Non-dimensional concentration as a function of non-dimensional time at the particle's surface for a constant flux $\delta = 0.2$.

Validation against numerical simulations.—Further validation is carried out by comparison with a finite difference based calculation for solid-phase diffusion in thin film, spherical particle, composite slab and composite spherical electrodes. In order to do so, a finite difference method is used. The governing equations and boundary conditions are discretized using an implicit approach. 1000 and 2000 nodes are used for single layer and double layer electrodes, respectively. A time-step of 1 s is used for the numerical solution. Mesh and time-step sensitivity study is carried out in order to ensure that the results are independent of these variables. Figures 4–7 present comparisons between the Green's function solution and numerical solution. Figure 4a plots concentration as a function of time for a linear time-dependent current density at the electrode's surface, $\delta(t) = A + B{\cdot}t$ for a thin film electrode for both analytical and numerical models. The concentration profile is plotted for a constant value of A and multiple values of slope, B. Very good agreement is seen for each case. Figure 4b plots the concentration as a function of distance, x, at multiple times for a linear current density, $\delta(t) = A + B{\cdot}t$, where A = −1 and B = −0.05. Note that the negative signs are due the discharge boundary condition. Similarly, for the same linear boundary condition, Figs. 5a and 5b plot the concentration as a function of time and distance for spherical electrode particle. Results show very good agreement between the two models.

Similar plots are shown in Figs. 6 and 7 for composite slab and spherical electrodes. The length of each layer in these composite electrodes are considered to be equal i.e. $l = 0.5$ and the ration of diffusion coefficient, α is considered to be 0.25. A linear dimensionless current density, $\delta(t) = A + B{\cdot}t$, is used as the boundary condition for both geometries. Figure 6a plots the concentration as a function of time at the electrodes surface for different values of slope, B for a composite slab electrode for both numerical and analytical models. Figure 6b plots the concentration as a function of distance at multiple times for the same case. Similarly, Figs. 7a and 7b plot concentration as a function of time at the electrode's surface and distance respectively for a composite spherical electrode for both numerical and analytical models. All plots show very good agreement between the analytical model and numerical simulation, thereby providing further validation in addition to the comparison.

Application of the model.—Following validation, the Green's function based model is used for analyzing a number of realistic problems involving time-dependent current density functions. Specifically, two different types of time-dependent flux boundary conditions are considered—sinusoidal and step functions. The first category not only covers periodic functions but also any arbitrary

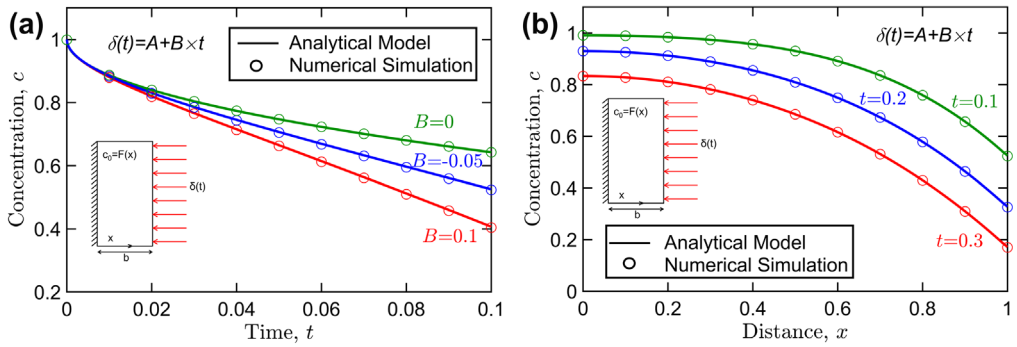

Figure 4. Validation against numerical model for a linear flux boundary condition, $\delta(t) = A + B{\cdot}t$ in a thin film electrode: (a) Non-dimensional concentration as a function of non-dimensional time at the electrode's surface for $A = -1$ and multiple values of slope, B, (b) Non-dimensional concentration as function of non-dimensional distance, x, for $A = -1$ and $B = -0.05$ at multiple times.

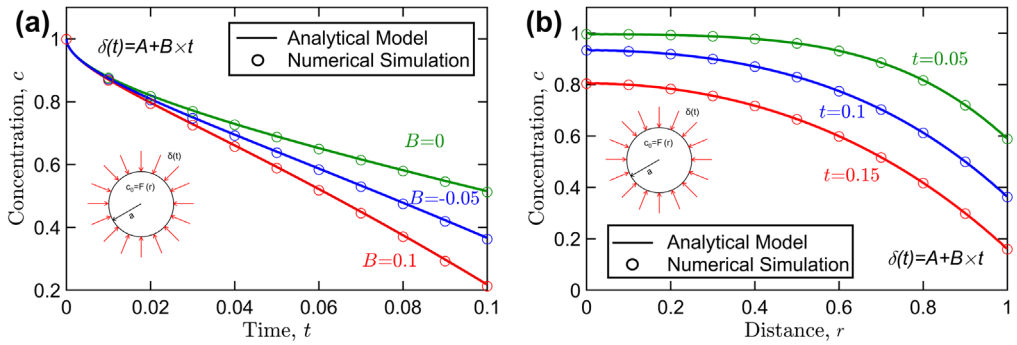

Figure 5. Validation against numerical model for a linear flux boundary condition, $\delta(t) = A + B{\cdot}t$ in a spherical electrode particle: (a) Non-dimensional concentration as a function of non-dimensional time at the electrode's surface for $A = -1$ and multiple values of slope, B, (b) Non-dimensional concentration as function of non-dimensional distance, r, for $A = -1$ and $B = -0.05$ at multiple times.

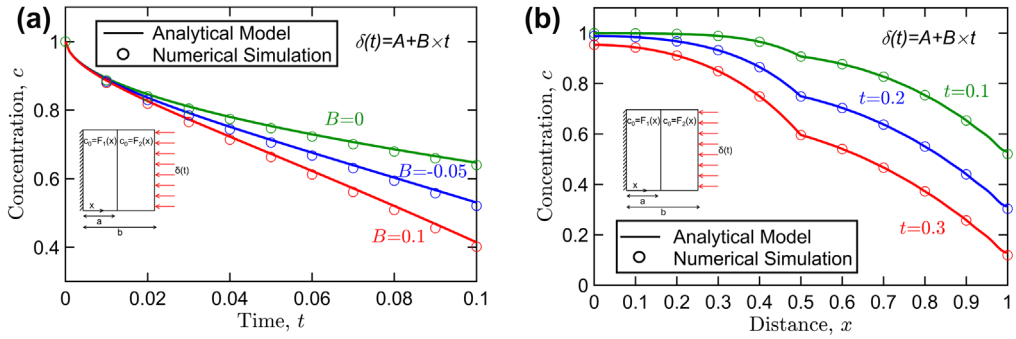

Figure 6. Validation against numerical model for a linear flux boundary condition, $\delta(t) = A + B{\cdot}t$ in a composite slab electrode: (a) Non-dimensional concentration as a function of non-dimensional time at the electrode's surface for $A = -1$ and multiple values of slope, B, (b) Non-dimensional concentration as function of non-dimensional distance, x, for $A = -1$ and $B = -0.05$ at multiple times.

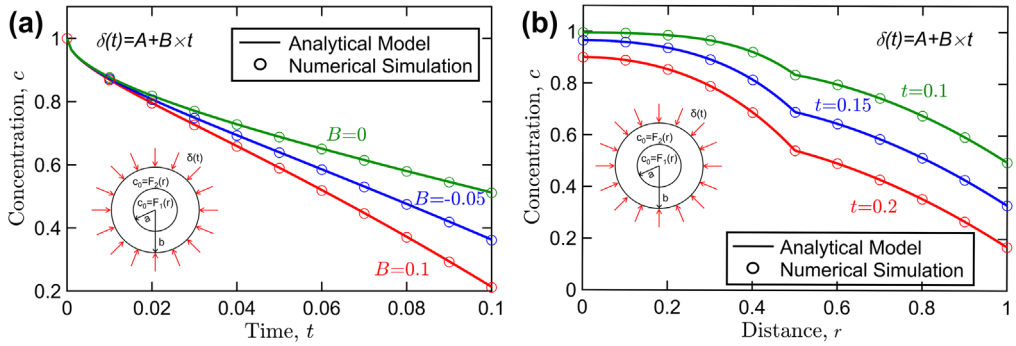

Figure 7. Validation against numerical model for a linear flux boundary condition, $\delta(t) = A + B{\cdot}t$ in a composite spherical electrode: (a) Non-dimensional concentration as a function of non-dimensional time at the electrode's surface for $A = -1$ and multiple values of slope, B, (b) Non-dimensional concentration as function of non-dimensional distance, r, for $A = -1$ and $B = -0.05$ at multiple times.

function since any appropriate function can be written as a series summation of periodic functions with different frequencies. Step functions can be used to address problems with sudden changes in C-rate during cyclic charge and discharge processes in Li-ion cells.

Figures 8a and 8b present plots for a non-dimensional time-dependent sinusoidal current density $\delta = 1 + \mathrm{Sin}(\omega t)$ with two different frequencies. Figure 8a plots concentration as a function of time at the surface of a spherical particle for $\omega = 100$, whereas Fig. 8b presents a similar plot for $\omega = 1000$. As expected, the concentration profile goes up and down with time at the expected frequency based on the value of ω. Figures 8a and 8b also present the results from a previous study Guo & White[37] which used an approximate solution for diffusion in spherical electrode particle under time-dependent boundary conditions. As seen from the figures, there is very good agreement between the present work and past paper,[37] with a worst-case deviation of 1.1% and 1% for data presented in Figs. 8a and 8b, respectively.

Figures 9a and 9b present spatial distributions of concentration for the same boundary conditions as Figs. 8a and 8b, respectively. Figure 9a and 9b plot concentration as a function of distance, r, at multiple times for $\omega = 100$ and $\omega = 1000$, respectively. As expected, the concentration is highest at the surface of the electrode since the flux is coming in at this location. Figure 9a shows that concentration increases rapidly between $t = 0$ and $t = 0.02$, corresponding to the time during which flux is high. Following that, the concentration close to the surface actually reduces for $t = 0.04$ and $t = 0.06$, beyond which, there is a sharp increase. This is consistent with flux as a function of time, as well as the surface concentration plot as a function of time shown in Fig. 8a. The corresponding concentration distribution plots for $\omega = 1000$ are, in comparison, monotonic, due to the larger frequency.

Figure 10 presents results for a discharge process with sinusoidal current density, $\delta(t) = A(1 + \sin \omega t)$ for multiple values of frequency, ω. Surface concentration is plotted as a function of time for

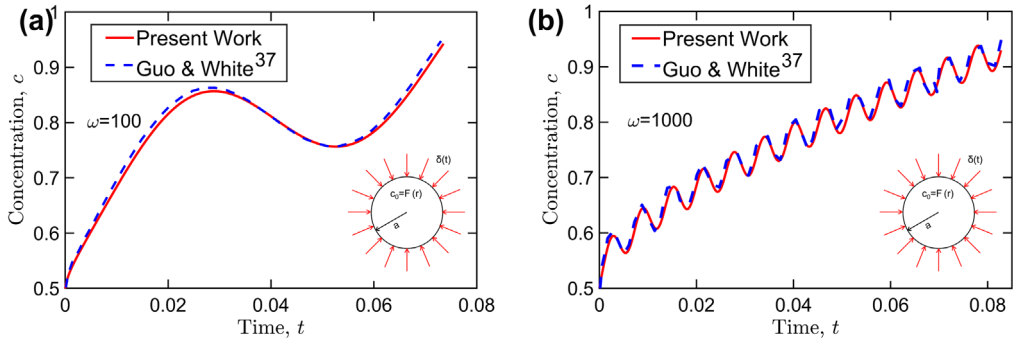

Figure 8. Non-dimensional concentration as a function of non-dimensional time at the surface of a spherical particle with sinusoidally varying flux, $\delta(t) = 1 + \sin(\omega t)$ for: (a) $\omega = 100$; (b) $\omega = 1000$. For comparison, plots from a past paper[37] are also shown.

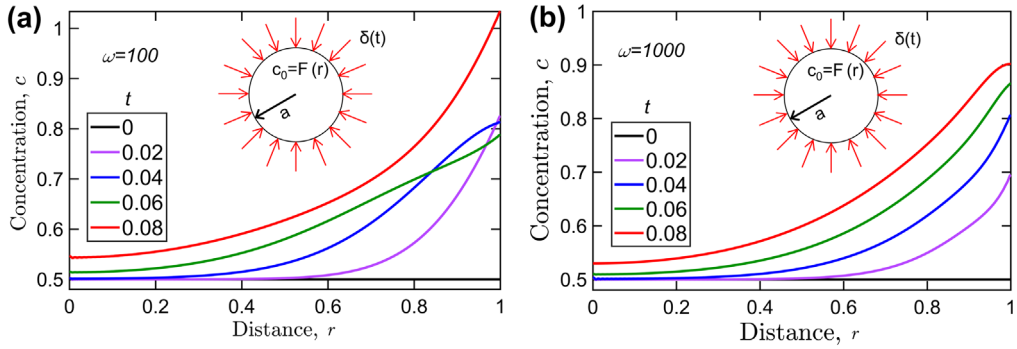

Figure 9. Non-dimensional concentration as a function of non-dimensional distance, r, at multiple times at the surface of a spherical particle with sinusoidally varying flux, $\delta(t) = 1 + \sin(\omega t)$ for: (a) $\omega = 100$; (b) $\omega = 1000$.

a thin film electrode and a spherical electrode particle in Figs. 10a and 10b, respectively. In both cases, the predicted concentration plot is consistent with the periodic nature of the forcing function. As expected, the concentration profile oscillates at the same frequency as the imposed current density, whereas the overall rate of reduction in the concentration is nearly the same for all cases.

Figure 11 presents plots for a scenario where the current density changes with time as a step function. This may be relevant where the C-rate of the cell changes due to changes in the external circuit, such as when an electric vehicle suddenly brakes or accelerates. Another practical scenario of relevance may be the cyclic charge and discharge of a Li-ion cell where the current density switches directions between charge and discharge periods. Two specific cases are considered. In the first case, the current density changes from a negative value of $\delta = -1$ at $t = 0.03$ to a positive value of $\delta = 0.5$, and then becomes negative ($\delta = -1.5$) again at $t = 0.05$. Figure 10a plots concentration as a function of time at the electrode's surface in a thin film electrode for this case. The current density is plotted as a function of time in the inset. Figure 10 shows that the concentration reduces during the discharge period, then increases rapidly during charge, and finally follows a downward trend again during the third phase of the process. The computational time associated with the calculations for Fig. 10 is relatively small (less than 30 s on a 3.30 GHz desktop computer with 8 GB RAM), since the eigenvalues depend only on the geometry and diffusivity, and need to be calculated only one time. Once the eigenvalues are calculated, they can be used to calculate the concentration profile under any types of boundary conditions. Therefore, the Green's function based model can be used for rapidly analyzing complicated, realistic charge/discharge scenarios.

Figure 11b plots the concentration profile as a function of time for a spherical electrode particle with a step-change current density. In this case, the current density function is a three-step function with values of $\delta = -0.5$, -1 and -1.5, as shown in the inset of Fig. 11b.

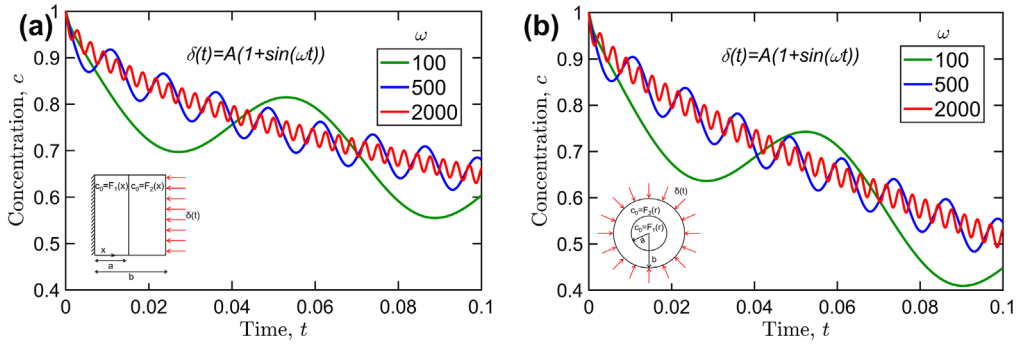

Figure 10. Practical application of the model in predicting concentration profile for a periodic flux boundary condition, $\delta(t) = A(1 + \sin(\omega t))$: Non-dimensional concentration as a function of non-dimensional time at the electrode's surface for $A = -1$ and multiple values of frequency, ω, for (a) a composite slab electrode (b) a composite spherical electrode.

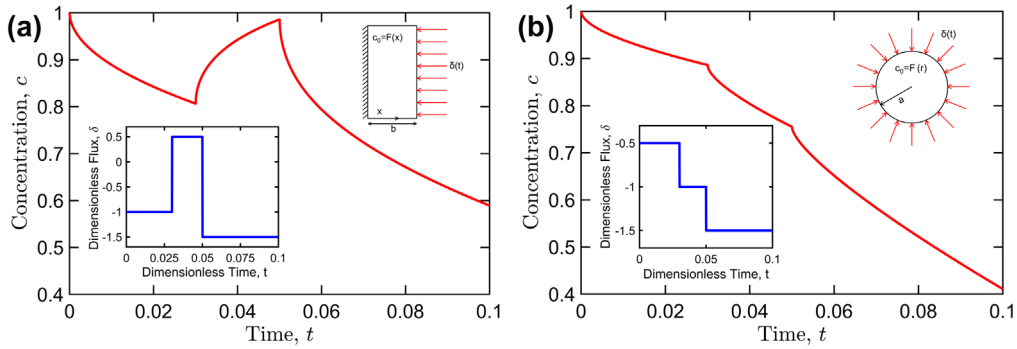

Figure 11. Practical application of the model in predicting concentration profile for step-change flux boundary conditions: Non-dimensional concentration as a function of non-dimensional time at the electrode's surface for (a) a charge-discharge process (b) a discharge process at different rates.

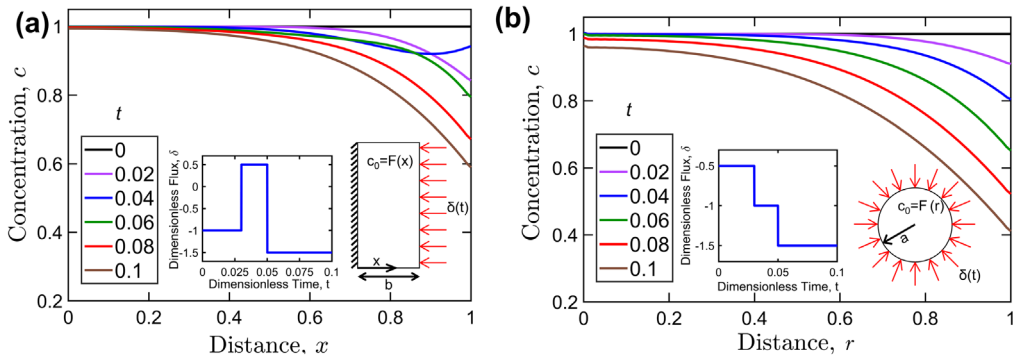

Figure 12. Practical application of the model in predicting concentration profile for step-change flux boundary conditions: Non-dimensional concentration as a function of non-dimensional distance, x and r, at multiple times at the electrode's surface for (a) a charge-discharge process (b) a discharge process at different rates.

This scenario may occur in applications with sudden changes in discharge rate. Figure 11b shows, as expected, a gradual reduction in concentration due to the negative current density. As the discharge current density increases in magnitude, concentration reduces more and more rapidly, as expected.

Figure 12 plots corresponding spatial concentration profiles at multiple times for the same parameters of step-function flux boundary condition as Fig. 11. Figure 12a shows that the concentration reduces, then increases, and then reduces, consistent with the variation of the flux boundary condition over time. Concentration at $r = 1$ is the highest at $t = 0.04$, which is because $t = 0.04$ lies in the region when the flux is positive. Concentration profiles in Fig. 12b are similarly consistent with the corresponding variation of flux with time.

Conclusions

In this paper, an exact solution is developed for solid-phase diffusion under a time-dependent flux boundary condition using the Green's function approach, which has been used widely in the past for solving thermal conduction problems. The method is first applied to a thin film electrode and a spherical electrode particle. The method is then extended to determine the concertation profile in two-layer slab and spherical composite electrodes. The mathematical models agree well with previous studies for specific cases, as well as numerical simulations. The Green's function-based model presented here is able to accurately predict the transient behavior during solid phase diffusion process relevant to a Li-ion cell. The Laplace transform approach used in previous studies provides separate expressions for short time and long solutions. The short time solution derived using Laplace transform, which is very useful for some applications such as high rates and short times may be calculated faster than the Green's function solution presented here, since there is no separate expression for short time solution using this method. However, for complicated flux boundary conditions, inversion of the Laplace solution may be challenging, whereas the present approach offers a closed-form solution. The model presented here can be used to predict the concentration profile under realistic time-dependent boundary conditions that may appear in practical applications for electrochemical energy storage.

Acknowledgments

This material is based upon work supported by CAREER Award No. CBET-1554183 from the National Science Foundation. Authors would like to gratefully acknowledge helpful discussions with Prof. Venkat Subramanian, Dr. Manan Pathak and Qiu Teo.

ORCID

Ankur Jain https://orcid.org/0000-0001-5573-0674

References

1. B. Scrosati and J. Garche, *J. Power Sources*, **195**, 2419 (2010).
2. J. B. Goodenough and K.-S. Park, *J. Am. Chem. Soc.*, **135**, 1167 (2013).
3. K. Shah et al., *Journal of Electrochemical Energy Conversion and Storage*, **14**, 020801(1) (2017).
4. B. Dunn, H. Kamath, and J.-M. Tarascon, *Science*, **334**, 928 (2011).
5. A. D. Pasquier, I. Plitz, S. Menocal, and G. Amatucci, *J. Power Sources*, **115**, 171 (2003).
6. B. A. Johnson and R. E. White, *J. Power Sources*, **70**, 48 (1998).
7. M. Parhizi, M. Ahmed, and A. Jain, *J. Power Sources*, **370**, 27 (2017).
8. A. Jokar, B. Rajabloo, M. Désilets, and M. Lacroix, *J. Power Sources*, **327**, 44 (2016).
9. R. Xiong, J. Cao, Q. Yu, H. He, and F. Sun, *IEEE Access*, **6**, 1832 (2018).
10. V. Ramadesigan et al., *J. Electrochem. Soc.*, **159**, A682 (2012).
11. A. Seaman, T.-S. Dao, and J. Mcphee, *J. Power Sources*, **256**, 410 (2014).
12. J. Zhang and J. Lee, *J. Power Sources*, **196**, 6007 (2011).
13. T. Hansen and C.-J. Wang, *J. Power Sources*, **141**, 351 (2005).
14. G. G. Botte, V. R. Subramanian, and R. E. White, *Electrochim. Acta*, **45**, 2595 (2000).
15. M. Doyle, *J. Electrochem. Soc.*, **140**, 1526 (1993).
16. V. Ramadesigan, V. Boovaragavan, J. C. Pirkle, and V. R. Subramanian, *J. Electrochem. Soc.*, **157**, A854 (2010).
17. V. R. Subramanian, V. Boovaragavan, V. Ramadesigan, and M. Arabandi, *J. Electrochem. Soc.*, **156**, A260 (2009).
18. G. Ning and B. N. Popov, *J. Electrochem. Soc.*, **151**, A1584 (2004).
19. S. Santhanagopalan, Q. Guo, P. Ramadass, and R. E. White, *J. Power Sources*, **156**, 620 (2006).
20. S. K. Rahimian, S. Rayman, and R. E. White, *J. Power Sources*, **224**, 180 (2013).
21. S. Atlung, *J. Electrochem. Soc.*, **126**, 1311 (1979).
22. M. Doyle and J. Newman, *J. Appl. Electrochem.*, **27**, 846 (1997).
23. V. R. Subramanian and R. E. White, *J. Power Sources*, **96**, 385 (2001).
24. B. Suthar and V. R. Subramanian, *J. Electrochem. Soc.*, **161**, E3149 (2014).
25. S. H. Ali, A. Hussin, and A. Arof, *J. Power Sources*, **112**, 435 (2002).
26. M. R. Johan and A. K. Arof, *Ionics*, **10**, 405 (2004).
27. S. Liu, *Solid State Ionics*, **177**, 53 (2006).
28. M. R. Johan and A. K. Arof, *J. Power Sources*, **170**, 490 (2007).
29. V. R. Subramanian, V. D. Diwakar, and D. Tapriyal, *J. Electrochem. Soc.*, **152** (2005).
30. V. R. Subramanian, J. A. Ritter, and R. E. White, *J. Electrochem. Soc.*, **148** (2001).
31. K. A. Smith, C. D. Rahn, and C.-Y. Wang, *J. Dyn. Syst. Meas. Control*, **130** (2008).
32. K. A. Smith, C. D. Rahn, and C.-Y. Wang, *Energy Convers. Manage.*, **48**, 2565 (2007).
33. D. D. Domenico, G. Fiengo, and A. Stefanopoulou, *2008 IEEE International Conference on Control Applications* (2008).
34. L. Cai and R. E. White, *J. Electrochem. Soc.*, **156**, A154 (2009).
35. W. Luo, C. Lyu, L. Wang, and L. Zhang, *Microelectron. Reliab.*, **53**, 797 (2013).
36. W. Luo, C. Lyu, L. Wang, and L. Zhang, *J. Power Sources*, **241**, 295 (2013).
37. M. Guo and R. E. White, *J. Power Sources*, **198**, 322 (2012).
38. Q. Zhang and R. E. White, *J. Power Sources*, **165**, 880 (2007).
39. D. W. Hahn and M. N. Özişik, *Heat Conduction* (Wiley, New York) (2012).
40. K. D. Cole, J. V. Beck, A. Haji-Sheikh, and B. Litkouhi, *Heat Conductions Using Greens Functions* (CRC Press, Boca Raton, FL) (2010).